Majorana corner pairs in a two-dimensional *s*-wave cold atomic superfluid

Ya-Jie Wu,[1,2] Xi-Wang Luo,[1] Junpeng Hou,[1] and Chuanwei Zhang[1,*]
[1]*Department of Physics, The University of Texas at Dallas, Richardson, Texas 75080-3021, USA*
[2]*School of Science, Xi'an Technological University, Xi'an 710032, China*

(Received 15 June 2020; revised 17 November 2020; accepted 7 December 2020; published 11 January 2021)

We propose a method to prepare Majorana pairs at the corners of imprinted defects on a two-dimensional cold-atom optical lattice with *s*-wave superfluid pairing. Different from previous proposals that manipulate the effective Dirac masses, our scheme relies on the sign flip of the spin-orbit coupling at the corners, which can be tuned in experiments by adjusting the angle of incident Raman lasers. The Majorana corner pairs are found to be located at the interface between two regimes with opposite spin-orbit coupling strengths in an anticlockwise direction and are robust against certain symmetry-persevered perturbations. Our work provides a way for implementing and manipulating Majorana pairs with existing cold-atom techniques.

DOI: 10.1103/PhysRevA.103.013307

I. INTRODUCTION

Majorana zero modes (MZMs) have attracted great attention in past decades owing to their non-Abelian exchange statistics and potential applications as topologically protected qubits [1,2]. They also exhibit significant physics in a range of disciplines such as nuclear and particle physics [3]. Strenuous efforts to search for MZMs are underway in both theories and experiments. In recent years, a variety of schemes to realize Majorana excitations have been proposed [4–18] by utilizing *p*-wave superconductors (SCs) or superfluid (SFs) [4,5], or SCs and SFs with effective *p*-wave paring via spin-orbit coupling (SOC) and *s*-wave pairing [6–10]. Remarkable experimental progress has been made in condensed-matter systems [19–24]. The experimental realization of SOC in ultracold atomic gases offer another clean platform to explore Majorana physics [25–31]. In these platforms the interplay among SOC, Zeeman fields, and *s*-wave interactions could produce non-Abelian topological superfluids (TSFs) that host Majorana excitations. There have been several tantalizing proposals for realizing and tuning Majorana excitations, for example, by creating topological defects (such as SF vortices or lattice dislocations) or one-dimensional defect regions [32,33].

The emergence of Majorana excitations can be intuitively understood by the low-energy theory. A pair of MZMs exists at the kinks where the pairing potential or SOC changes sign (which corresponds to the sign change of Dirac mass or velocity in the Jackiw-Rebbi model). In solid-state materials, the SOC kinks are difficult to tune, while the kinks of pairing potentials can be realized through Josephson junctions in superconducting nanowires, as well as the corners and hinges in recently proposed higher-order topological SCs (TSCs) [34–47]. In particular, for two-dimensional (2D) second-order TSCs, the bulk topology of the 2D system offers one-dimensional (1D) edge modes, which have different topologies for adjacent edges due to the change of the pairing sign, leading to zero-energy Majorana Kramers pairs or Majorana modes at corners [42–45]. On the other hand, in cold atomic system, the kinks of pairing potentials may be obtained by soliton excitations [48–50]. However, these cold atomic systems suffer from dynamical instability in the presence of perturbations. Thus proposals for realizing robust MZMs in atomic systems, through other manners like SOC kinks, are highly in demand.

In this paper we propose feasible schemes to realize SOC kinks using trapped ultracold fermionic atoms on a 2D optical lattice and show that our system supports Majorana pairs in a vortex-free configuration. The main results are listed below:

(i) Effective 1D modes on a rectangular geometry would emerge in the 2D system through engineering on-site potential of the outer rectangular region. In the presence of 1D equal Rashba-Dresselhaus (ERD) SOCs, Majorana corner pair emerges at the corner of the rectangle with a proper *s*-wave pairing.

(ii) Each edge of the rectangular defect is characterized by a 1D topological SF in the chiral orthogonal (BDI) class, and a Majorana pair exists at the interface of two adjacent edges which has different signs of SOC (clockwise or anticlockwise along the defective geometry). Our system is in analog with the higher-order TSCs, except that the low-energy 1D model is induced by the outer rectangular region rather than the bulk topology, and the MZMs are induced by SOC kinks rather than pairing kinks between two adjacent boundaries [42,43]. Our system is more concise and experimentally friendly, since no tricky unconventional pairings, like *d* wave or $s_{\pm}$ wave, are required.

(iii) Our system can be realized with currently already established experimental techniques in cold atoms, including 1D ERD SOC by Raman lasers [25,26], single-site addressing in 2D optical lattices [51–55], and tunable *s*-wave interaction through Feshbach resonance [56,57].

*chuanwei.zhang@utdallas.edu

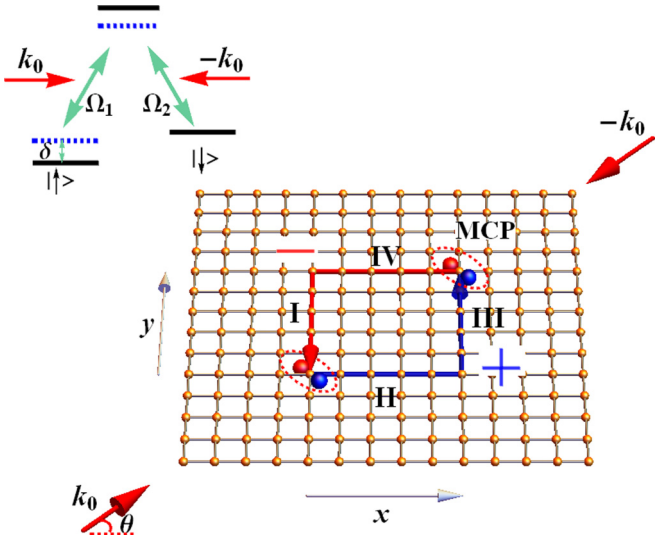

FIG. 1. Illustration of system setup on a 2D optical lattice, where two counterpropagating Raman beams are incident with angle θ. A dip potential is applied on a rectangle geometry (indicated by the blue and red curves) through single-site addressing. Under the configuration $\theta = \pi/4$, the sign of effective SOC is positive (+)/negative (−) on the blue/red lines in edge coordinate along the arrows. Two spheres (encircled by the red dashed oval) at the interface denote the Majorana corner pair (MCP). The inset above shows the level diagram.

(iv) The Majorana corner pair is robust against shape deformation of the defective rectangle, even to the extent of a defective loop. In addition, the SOC direction dictates on which corners the Majorana pair resides. Therefore the incident direction of Raman lasers can be used to manipulate Majorana pairs.

The paper is organized as follows. In Sec. II we first introduce the Hamiltonian with 1D ERD SOC on optical lattices and obtain the phase diagram consisting of metal and s-wave SF phases. In Sec. III, we study the case with a defective outer rectangular region and find Majorana pairs emerge at the corners. We extend the discussion to a ring-shaped geometry in Sec. IV, where Majorana pairs arise naturally due to soft domain walls of SOC. Finally, we make conclusions and discussions in Sec. V.

II. SPIN-ORBIT-COUPLED s-WAVE SUPERFLUIDS ON 2D OPTICAL LATTICES

We utilize atomic hyperfine states as the pseudospin states $|\uparrow\rangle$ and $|\downarrow\rangle$, as illustrated in Fig. 1. The SOC is synthesized by two counterpropagating Raman lasers coupling the two hyperfine states. The single-atom motion in 2D real space is described by the Hamiltonian $\hat{H}_{0,a} = \frac{\vec{k}^2}{2m_0} + \frac{\delta}{2}\sigma_z + (\Omega e^{2i\vec{k}_0\cdot\vec{r}}|\downarrow\rangle\langle\uparrow| + \text{H.c.})$, where the reduced Planck constant $\hbar$ has been set to be 1, $\Omega \propto \Omega_1\Omega_2^*$ is the strength of Raman coupling, and $\vec{k}_0 = k_{0,x}\vec{e}_x + k_{0,y}\vec{e}_y$ is the wave vector of the Raman laser. The off-diagonal terms correspond to a spin-flip process accompanied by a momentum transfer of $2\vec{k}_0$, describing the SOC effects. The detuning term reads $\delta = \omega_z - \delta\omega$, where $\omega_z > 0$ is the energy difference between these two hyperfine states, and $\delta\omega$ denotes the frequency difference between two Raman laser beams. In the following we assume that other hyperfine levels are far off-resonance under the two-phonon process, for example, by quadratic Zeeman shift. The Hamiltonian is first transformed by a unitary matrix, namely, $\hat{H}_{0,b} = U\hat{H}_{0,a}U^{-1}$, where $U = \text{diag}(e^{-i\vec{k}_0\cdot\vec{r}}, e^{i\vec{k}_0\cdot\vec{r}})$. We then perform other pseudospin rotations $\tilde{U} = e^{-i\frac{\pi}{4}\sigma_z}e^{-i\frac{\pi}{4}\sigma_y}$ to obtain $\hat{H}_0 = \tilde{U}\hat{H}_{0,b}\tilde{U}^\dagger$, which can be written as

$$\hat{H}_0 = \frac{1}{2m_0}[(k_x + k_{0,x}\sigma_y)^2 + (k_y + k_{0,y}\sigma_y)^2] + \frac{\delta}{2}\sigma_y - \Omega\sigma_z. \tag{1}$$

The Raman transition produces a desired ERD SOC. In the following we assume $\delta = 0$ for convenience.

The 1D system suffers from strong quantum fluctuations, which could eliminate s-wave SF order, together with the Majorana modes. This motivates us to investigate the physics in 2D, where quasi-long-range SF order exists below the Berezinskii-Kosterlitz-Thouless (BKT) transition temperature. We concentrate on the lowest (nearly) degenerate bands for constructing a tight-binding model. From Eq. (1), through the operator $\hat{\Psi}(\vec{r}) = \sum_{i,\sigma}\hat{c}_{i,\sigma}\psi_\sigma(\vec{r} - \vec{r}_i)$ with $\psi_\sigma(\vec{r} - \vec{r}_i)$ the Wannier function at site i, we obtain a second-quantization formula:

$$\hat{H}_{0s} = \sum_i \big(-t_x\hat{c}_i^\dagger\hat{c}_{i+e_x} - t_y\hat{c}_i^\dagger\hat{c}_{i+e_y} - it_{\text{sox}}\hat{c}_i^\dagger\sigma_y\hat{c}_{i+e_x} - it_{\text{soy}}\hat{c}_i^\dagger\sigma_y\hat{c}_{i+e_y}\big) + \text{H.c.} - h_z\hat{c}_i^\dagger\sigma_z\hat{c}_i - \mu\hat{c}_i^\dagger\hat{c}_i, \tag{2}$$

where $t_x = t_0\cos(k_0\cos\theta)$, $t_y = t_0\cos(k_0\sin\theta)$, $t_{\text{sox}} = t_0\sin(k_0\cos\theta)$, $t_{\text{soy}} = t_0\sin(k_0\sin\theta)$, and the bare hopping strength reads $t_0 = -\int d\vec{r}\psi_\sigma^*(\vec{r} - \vec{r}_i)(\frac{k_x^2+k_y^2}{2m_0} + V_{\text{lat}})\psi_\sigma(\vec{r} - \vec{r}_{i+1})$. Here we have chosen the basis $\hat{c}_i = (\hat{c}_{i,\uparrow}, \hat{c}_{i,\downarrow})^T$ and denoted $h_z = \Omega$. The incident angle θ is illustrated in Fig. 1. The lattice spacing is set to be $a = 1$. Hereafter, we set $t_0 = 1/\cos[k_0\sin(\pi/4)] = 1/\cos(\sqrt{2}\pi/4)$ for convenience. When $\theta = \pi/4$, we have approximately $t_{\text{sox}} = t_{\text{soy}} \approx 2t_x = 2t_y$.

We consider an attractive SU(2)-invariant interaction $\hat{H}_{int} = -\sum_i U\hat{n}_{i,\uparrow}\hat{n}_{i,\downarrow}$ and study the superfluid phase under mean-field approach by solving the s-wave superfluid order parameter $\Delta_s = U\langle c_{i,\downarrow}c_{i,\uparrow}\rangle$ self-consistently. The Bogoliubov–de Gennes (BdG) Hamiltonian in the Nambu basis $\Psi_k = (c_{k\uparrow}, c_{k\downarrow}, c_{-k\downarrow}^\dagger, -c_{-k\uparrow}^\dagger)^T$ is described by $\hat{H}_s = \sum_k \Psi_k^\dagger H(k)\Psi_k$ with

$$H(k) = (\epsilon_k + \gamma_k\sigma_y)\tau_z - h_z\sigma_z + \Delta_s\tau_x, \tag{3}$$

where $\epsilon_k = -2(t_x\cos k_x + t_y\cos k_y) - \mu$, $\gamma_k = 2(t_{\text{sox}}\sin k_x + t_{\text{soy}}\sin k_y)$, and σ and τ are Pauli matrices acting on the spin and particle-hole spaces, respectively. By minimizing free energy with respect to the order parameter Δ_s and chemical potential μ, we may derive the following self-consistent equations:

$$1 = \frac{U}{2N_l}\sum_{\nu=\pm,k}\frac{\tanh(\beta\xi_{k,\nu}/2)}{\xi_{k,\nu}}\left(1 + \frac{\nu h_z^2}{g_k}\right), \tag{4}$$

$$n_f = 1 - \frac{1}{N_l}\sum_{\nu=\pm,k}\epsilon_k\frac{\tanh(\beta\xi_{k,\nu,}/2)}{\xi_{k,\nu}}\left(1 + \frac{\nu m_k^2}{g_k}\right), \tag{5}$$

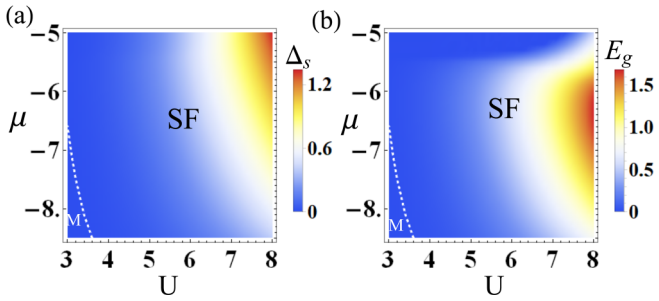

FIG. 2. (a) SF order parameter Δ_s vs interaction U and chemical potential μ. A phase transition occurs between metal (M) and superfluid (SF) phases. (b) Similar as panel (a) but plotted with Bogoliubov quasiparticle energy gap E_g. In both panels we take $t_x = t_y = 1$, $t_{\rm sox} = t_{\rm soy} = 2$, $h_z = 1.4$.

where n_f is the particle filling factor, N_l is the number of lattice sites, and other parameters are defined as $\beta = 1/(k_B T)$, with k_B the Boltzmann constant and T the temperature, $\xi_{k,v=\pm} = \sqrt{\epsilon_k^2 + \Delta_s^2 + m_k^2 + 2v g_k}$, $g_k = \sqrt{\epsilon_k^2 m_k^2 + \Delta_s^2 h_z^2}$, and $m_k = \sqrt{h_z^2 + |\gamma_k|^2}$. By numerically solving Eqs. (4) and (5), we obtain phase diagrams at zero temperature for pairing order Δ_s and quasiparticle energy gap E_g in Figs. 2(a) and 2(b), respectively. Figure 2(a) confirms the phase transition from a metal (M) phase to an s-wave SF. From panel (b) we find a finite gap for Bogoliubov quasiparticle excitations in the proper parameter region in the SF phase. The energy gap also survives on a finite-size sample and could protect Majorana modes from lower extended states.

III. MAJORANA CORNER PAIRS ON A TOPOLOGICAL DEFECTIVE RECTANGULAR GEOMETRY

Given a proper local dip potential, the one-dimensional defect region enjoys a nontrivial topology belonging to the BDI class. It can be characterized through a winding number, which is discussed in Appendix A. Similarly, with a local dip μ_d, we can get a defective outer rectangular region in the 2D optical lattice as illustrated in Fig. 1, where SOC domain walls (anticlockwise or clockwise) naturally arise at two corners. In the following we will first focus on the continuum limit to explore the nature of the emerged Majorana pairs, supplemented with self-consistent numerical calculations on a 2D optical lattice.

We assume that with appropriate μ_d, the outer rectangular region enters the TSF phase while the rest remains trivial. As a result, we could assume that the topological outer rectangular region is isolated from the 2D bulk. The numerics performed on a 2D optical lattice with an imprinted defective rectangular outer region also supports this assumption later. From Eq. (3) the low-energy Hamiltonian expands around $\vec{k} = (0, 0)$ on edges m = I, II, III, IV (see Fig. 1) and is then given by

$$H_{\rm m} = t_{\rm m} k_{\rm m}^2 \tau_z + 2t_{s,{\rm m}} k_{\rm m} \sigma_y \tau_z - \mu_{\rm m} \tau_z - h_z \sigma_z + \Delta_{s,{\rm m}} \tau_x, \quad (6)$$

where $t_{\rm I} = t_{\rm III} = t_y$, $t_{\rm II} = t_{\rm IV} = t_x$, $k_{\rm I} = k_{\rm III} = k_y$, $k_{\rm II} = k_{\rm IV} = k_x$, $t_{s,{\rm I}} = t_{s,{\rm III}} = 2t_{\rm soy}$, and $t_{s,{\rm II}} = t_{s,{\rm IV}} = 2t_{\rm sox}$. The on-site chemical potential is $\mu_{\rm m} = \mu + 2(t_x + t_y) - \mu_d$, with μ_d the dip potential and $\Delta_{s,{\rm m}}$ the s-wave pairing on each edge. Without loss of generality, we set incident angle of Raman lasers $\theta = \frac{\pi}{4}$ such that $t_x = t_y = t$, $t_{\rm sox} = t_{\rm soy} = t_{\rm so}$, $\mu_{\rm m} = \mu_{\rm edge} = \mu + 4t - \mu_d$, and assume the s-wave SF order parameter is nearly uniform on the four edges $\Delta_{s,{\rm m}} = \Delta_{\rm edge}$. For later convenience, we take an "edge coordinate" s, in which we take the anticlockwise direction as positive. In such a coordinate, the low-energy edge Hamiltonian reads

$$H_{\rm edge} = -t\tau_z \frac{\partial^2}{\partial s^2} - i\alpha(s)\sigma_y \tau_z \frac{\partial}{\partial s} - \mu_{\rm edge}\tau_z - h_z \sigma_z + \Delta_{\rm edge}\tau_x, \quad (7)$$

with $\alpha(s) = -2t_{\rm so}$, $2t_{\rm so}$, $2t_{\rm so}$, $-2t_{\rm so}$ for edges I–IV, respectively. Remarkably, while the terms $\Delta_{\rm edge}$ and $\mu_{\rm edge}$ remain the same on the four edges, the effective coupling $\alpha(s)$ changes sign at two of the four corners [the corner between the edges I (III) and II (IV)], forming two SOC domain walls as illustrated in Fig. 1. This will give rise to a Majorana pair if $h_z^2 > \mu_{\rm edge}^2 + \Delta_{\rm edge}^2$. Specifically, at the corner between edges I and II (corner $s = 0$ in our coordinate), two orthogonal wave functions for MCMs are given by

$$\Psi_{0,\pm} = C_\pm e^{-\eta_\pm |s|} \left(e^{i\frac{\phi_\pm}{2}} |y_+\rangle_\sigma |y_\pm\rangle_\tau + e^{-i\frac{\phi_\pm}{2}} |y_-\rangle_\sigma |y_\mp\rangle_\tau \right). \quad (8)$$

Here $C_\pm$ are normalization constants and $e^{i\phi_\pm} = \frac{h_z[i(\alpha\eta_\pm \mp \Delta_{\rm edge}) - (t\eta_\pm^2 + \mu_{\rm edge})]}{(t\eta_\pm^2 + \mu_{\rm edge})^2 + (\alpha\eta_\pm \mp \Delta_{\rm edge})^2}$, where $\eta_\pm = \frac{1}{2}\sqrt{-\frac{2\varkappa}{3} + \delta \mp \frac{1}{2}\sqrt{-\frac{4\varkappa}{3a} - \delta + \zeta_\pm}} > 0$, $\zeta_\pm = \mp 2d/(a\sqrt{-2c/(3a) + \delta}$, $\delta = \frac{\sqrt[3]{2}\delta_1}{3a\sqrt[3]{\delta_2 + \sqrt{-4\delta_1^3 + \delta_2^2}}} + \frac{\sqrt[3]{\delta_2 + \sqrt{-4\delta_1^3 + \delta_2^2}}}{3\sqrt[3]{2a}}$, $\delta_1 = \varkappa^2 + 12ae$, $\delta_2 = 2\varkappa^3 + 27ad^2 - 72a\varkappa e$, $a = t^2$, $\varkappa = \alpha^2 + 2t\mu_{\rm edge}$, $d = -2\alpha\Delta_{\rm edge}$, and $e = \Delta_{\rm edge}^2 - h_z^2 + \mu_{\rm edge}^2$. The vectors $|y_\pm\rangle_\sigma$ and $|y_\pm\rangle_\tau$ are eigenstates of operators σ_y and τ_y, respectively. Following a similar approach, we could also find two Majorana modes at the corner between edges III and IV (see Appendix B for details). We emphasize that as long as the four edges are in the TSF phase, the very existence of Majorana pairs is robust against the fluctuations of chemical potential and the SF order parameter.

With the above understanding of continuum systems, we now proceed to study the discrete cases on an optical lattice shown in Fig. 1. The total Hamiltonian now becomes

$$\hat{H}_{\rm BdG} = \hat{H}_s + \sum_{i \in \square} \mu_d \hat{c}_i^\dagger \hat{c}_i, \quad (9)$$

where $i \in \square$ enumerates each site with the dip potential (a rectangular geometry in this case). The local s-wave superfluid order parameter in real space is determined in a self-consistent manner [15], as well as the quasiparticle energy spectra and wave functions. On the defective outer rectangular region, the system is topological once $h_z > \sqrt{\tilde{\mu}^2 + \Delta_s^2}$ and $\tilde{\mu} = \mu + 2t_x + 2t_y - \mu_d$. In our self-consistent numerical calculations, we take the lattice sizes $n_x = n_y = 30$ and the sizes of outer rectangular region $n_x^d = n_y^d = 22$. The SF order parameter $\Delta_{s,i}$ is shown in Fig. 3(a), which has a constant phase across the entire system. Figure 3(b) shows the quasiparticle energy spectrum, where four Majorana bound states (two Majorana corner pairs) exist in the energy gap. A small energy splitting is observed as a result of the finite-size effect. Figure 3(c) shows the density distribution of the bounded Majorana corner states, which

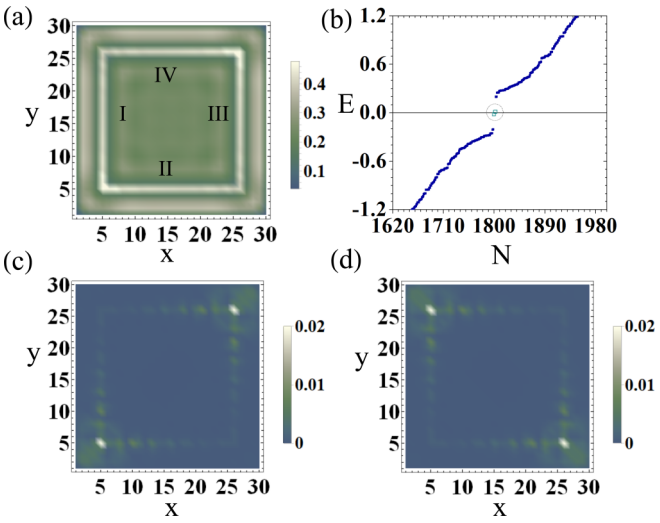

FIG. 3. (a) Self-consistent s-wave pairing order parameters in real space. (b) Energy-level diagrams. (c), (d) The real-space distributions of MZMs. For all panels we choose $t_x = t_y = 1$, $t_{\rm sox} = t_{\rm soy} = 2$, $\mu = -7.95$, $\mu_d = -4.0$, $h = 1.4$, $U = 6.3$. The incident angle is $\theta = \pi/4$ in (a)–(c) and $\theta = -\pi/4$ in (d).

clearly demonstrates its localization at the corners of the outer rectangular region.

The outer rectangular region of our system corresponds a 1D topological model in BDI class characterized by a $\mathbb{Z}$ topological invariant, which can support many zero Majorana modes in principle. The Majorana corner modes emerge since the corner is the intersection of two 1D topological chains with opposite winding numbers $w = \pm 1$, leading to $\Delta w = 2$ zero modes. They are protected by the underlying generalized time-reversal (with $\mathcal{T}^2 = 1$), particle-hole, and chiral symmetry in the one-dimensional region. The Majorana pairs here are different from the previous time-reversal symmetry ($\mathcal{T}^2 = -1$) protected Majorana Kramers pair in the $\mathbb{Z}_2$ topological class.

The incident angle of Raman lasers can change the SOC and the nearest-neighbor hopping, and thus alter the Majorana bound states. Figures 4(a) and 4(b) illustrate the corresponding phase diagram with respect to μ-θ and μ_d-θ, where Majorana corner pairs exist in the topological region (T). It is found that the Majorana pairs are also robust to certain

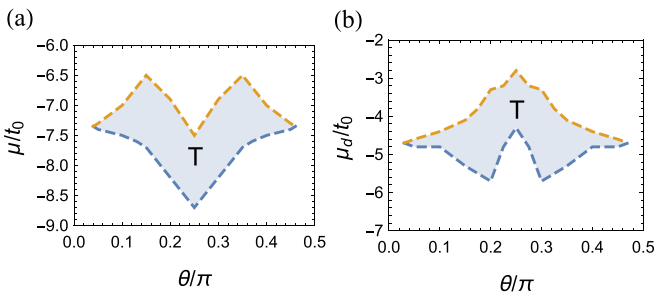

FIG. 4. Phase diagram for 2D system with the defective outer rectangular region. In region "T," Majorana bound states exist at corners. In (a), $\mu_d = -4.0$, $h_z = 1.4$, $U = 6.3$ are used. In (b), $\mu = -7.8$, $h_z = 1.4$, $U = 6.3$ are used.

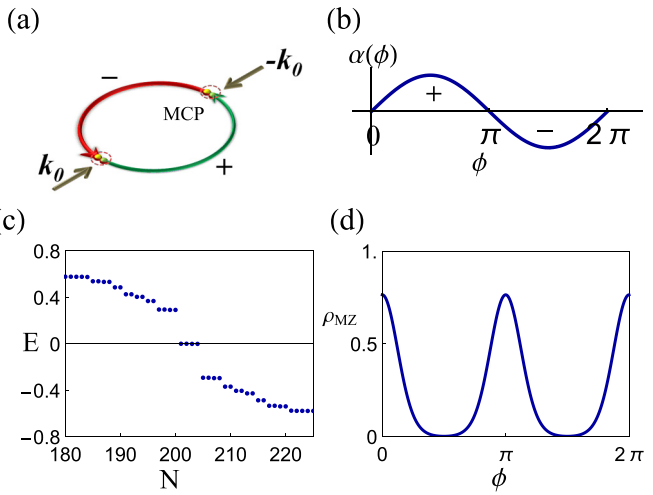

FIG. 5. (a) Illustration of a ring trap in which the atoms are confined. Two counterpropagating Raman lasers with wave vector $\pm\vec{k}_0$ couple the atomic hyperfine states. The notations + and − indicate the sign of SOC. Two spheres encircled by the red dashed circle denote a MCP. (b) The SOC term $\alpha(\phi)$ plotted to varying polar angle ϕ. (c) The eigenspectrum computed through plane-wave expansion. (d) The particle density $\rho_{\rm MZ}$ of Majorana zero modes vs the angle ϕ. The parameters are chosen as $\tilde{\alpha}_0 = 0.04$, $\eta = 0.005$, $\mu' = 0.2$, $h_z = -1.4$, $\Delta_s = 0.8$.

variation of the incident angle θ. We remark that if the sign of θ is reversed, the Majorana pairs appear at another two corners (the interfaces of II–III and I–IV), as shown in Fig. 3(d), which can be compared with Fig. 3(c). Thus our proposed setup provides better tunability for manipulating Majorana bound states.

If we consider a harmonic trap with the lowest potential energy at the center of the defect rectangle, the corner region would first enter the topologically trivial phase, and the defect rectangle was divided into four topological 1D lines (one on each edge of the defect rectangle). Each topological line hosts two Majorana bound states. Due to hybridization of Majorana modes within each topological line, there exist eight bound states with finite energy.

IV. MAJORANA CORNER PAIRS ON A RING GEOMETRY

In this section we study the case with a ring-shaped defect line. Here the optical lattice is removed, and we focus on the low-energy effective 1D model for simplicity. The effective model is illustrated in Fig. 5(a) and we find that soft domain walls of SOC naturally arise on the ring, which leads to the emergence of Majorana corner pairs.

Without loss of generality, we assume the momentum kick by Raman lasers is along the x direction. Under a spin rotation $\sigma_y \to \sigma_x$ with $k_{0,y} = 0$ in Eq. (1), the SOC has the form $\alpha_0 k_x \sigma_x$, where the coupling constant is given by the ratio of the laser wave vector and atomic mass, i.e., $\alpha_0 = k_0/m_0$. Hence in the continuum limit the effective Hamiltonian reads

$$\mathcal{H} = \frac{k^2}{2m_0}\tau_z + \alpha_0 k_x \sigma_x \tau_z - \mu\tau_z + h_z\sigma_z + \Delta_s\tau_x, \qquad (10)$$

where Δ_s is an s-wave SF order. For simplicity, we set Δ_s to be real. The relation $h_z > \sqrt{\mu^2 + \Delta_s^2}$ holds in the topological regions.

In a polar coordinate (ρ, ϕ), the above Hamiltonian becomes a function of polar angle ϕ on a ring with given radii ρ, i.e.,

$$\mathcal{H}(\phi) = -\eta\partial_\phi^2\tau_z + i\tilde{\alpha}_0 \sin\phi \frac{\partial}{\partial\phi}\sigma_x\tau_z - \mu'\tau_z + h_z\sigma_z + \Delta_s\tau_x, \tag{11}$$

where $\eta = \frac{1}{2m_0\rho^2}$, $\tilde{\alpha}_0 = \frac{\alpha_0}{\rho}$, and $\mu' = \mu - \frac{k_0^2}{2m_0}$ (more details are discussed in Appendix C). The Hamiltonian $\mathcal{H}(\phi)$ has particle-hole symmetry $\mathcal{P}\mathcal{H}(\phi)\mathcal{P}^{-1} = -\mathcal{H}(-\phi)$, where $\mathcal{P} = \sigma_y\tau_y\mathcal{K}$ and $\mathcal{K}$ denotes the complex conjugation. It also preserves a generalized time-reversal symmetry $\mathcal{T}\mathcal{H}(\phi)\mathcal{T}^{-1} = \mathcal{H}(-\phi)$ with $\mathcal{T} = \sigma_z\mathcal{K}$. The combination of $\mathcal{P}$ and $\mathcal{T}$ leads to the chiral symmetry $\mathcal{C}$: $\mathcal{C}\mathcal{H}(\phi)\mathcal{C}^{-1} = -\mathcal{H}(\phi)$, with $\mathcal{C} = \mathcal{P}\mathcal{T} = i\sigma_x\tau_y$. Therefore the Hamiltonian belongs to BDI class and can be characterized by a $\mathbb{Z}$ topological invariant [58,59].

In Eq. (11) the SOC $\alpha(\phi) = \tilde{\alpha}_0 \sin\phi$ changes sign at $\phi = 0, \pi$, as shown in Fig. 5(b). Specifically, we have $\alpha(\phi) > 0$ if $\phi \in (0, \pi)$ and $\alpha(\phi) < 0$ if $\phi \in (\pi, 2\pi)$. Hence the system can be divided into two segments. Both belong to the BDI class but possess opposite topological invariant. The interfaces are determined by $\phi = 0$ and π, corresponding to two "soft" domain walls in the sense that the SOC term changes smoothly across these two points. From Eq. (11), the Hamiltonian $\mathcal{H}(\phi)$ is invariant under a $2n\pi$ rotation if n is an integer. Therefore to solve the eigenvalues of $\mathcal{H}(\phi)$, we assume the following trial solution:

$$\Phi(\phi) = (u_a(\phi), \quad u_b(\phi), \quad u_c(\phi), \quad u_d(\phi))^T, \tag{12}$$

where $u_{v=a,b,c,d}(\phi) = \sum_m v_m e^{im\phi}$ and m is an integer. By solving the Schrödinger equation $\mathcal{H}(\phi)\Phi(\phi) = E\Phi(\phi)$, the eigenvalues are obtained as shown in Fig. 5(c). See Appendix C for more details. It is clear that four Majorana modes emerge (with an numerical error about $E \approx 10^{-4}$). One Majorana corner pair consisting of two Majorana modes localizes at $\phi = 0$, and the other pair localizes at $\phi = \pi$, as illustrated in Fig. 5(a). This is also demonstrated by the particle density distribution ρ_{MZ} of Majorana modes, as shown in Fig. 5(d). We remark that a toroidal Bose-Einstein condensate has been created in an all-optical trap [60]. We expect our scheme could be reached with similar techniques and additional Raman lasers.

V. DISCUSSION AND CONCLUSION

From the effective low-energy theory of TSFs, it is well known that Majorana modes would emerge if the sign of the Dirac mass changes, and most previous proposals are based on this principle. In this paper we propose an alternative approach to implement Majorana modes (Majorana corner pairs) through tuning the effective SOC. By loading Fermi gases on 2D optical lattices subjected to a 1D ERD SOC, we can find a SF phase under appropriate s-wave interaction and Zeeman field. Using single-site addressing techniques, we could engineer defective geometries, which are topologically nontrivial, on the 2D optical lattice. From the viewpoint of low-energy theories, an outer rectangular region consists of two TSFs characterized by distinct topological invariants whose sign is determined by the sign of SOC in edge coordinate. Obviously, the sign of SOC changes at two corners on the outer rectangular region. At the interface of two distinct TSFs, a topologically protected Majorana pair (two Majorana modes) naturally arises according to the index theorem. For TSF with 1D ERD SOC on a ring, two soft SOC domain walls exist, and two Majorana pairs also appear near the domain walls. In principle, as long as two effective 1D SFs are topological with different topological invariants $w = \pm 1$, the Majorana pair ($\Delta w = 2$ Majorana modes) will emerge at the interface. It is robust as long as the perturbations preserve three underlying symmetries $(\mathcal{P}, \mathcal{T}, \mathcal{C})$ of the system.

We emphasize that the Majorana corner pair in the context differs from those in second-order TSCs in two dimensions. First, for second-order TSCs with time-reversal symmetry [42,43], 1D edge modes evolve from the higher-dimensional bulk of the topological insulators. However, in our scheme the 1D modes originate from the defect geometry. Second, in a higher-order TSC, a momentum-dependent SC pairing ($s_\pm$ or d-wave) leads to a Dirac mass kink at the corner of the sample and then induces the Majorana Kramers pair. In contrary, our proposal utilizes the sign reversal of effective SOC on the edges and lacks Kramers degeneracy.

In summary, we propose a distinct scheme to implement Majorana pairs in an atomic platform. The coordinate of the Majorana pair depends on the position of the SOC domain wall, which can be tuned by the directions of the Raman laser beams. Moreover, our system is free of dynamical instability such that the MZM has a longer lifetime. Our work opens the possibility of implementing robust Majorana pairs and the associated non-Abelian braiding in cold atoms.

ACKNOWLEDGMENTS

This work is supported by Air Force Office of Scientific Research (FA9550-16-1-0387, FA9550-20-1-0220), the National Science Foundation (PHY-1806227), and the Army Research Office (W911NF-17-1-0128). This work is also supported in part by the NSFC under Grant No. 11504285, and the Scientific Research Program funded by the Natural Science Basic Research Plan in Shaanxi Province of China (Program No. 2018JQ1058), the Scientific Research Program funded by the Shaanxi Provincial Education Department under Grant No. 18JK0397, and a scholarship from the China Scholarship Council (CSC) (Program No. 201708615072).

APPENDIX A: MAJORANA MODES AT THE ENDS OF TOPOLOGICAL DEFECTIVE CHAIN

In this section we show how a topologically nontrivial defective chain can be implemented through on-site potential engineering on 2D optical lattices. For a 1D system with SOC and SF order, the system is topological if $h_z > \sqrt{(\tilde{\mu} - \mu_d)^2 + \Delta_s^2}$, where $\tilde{\mu} = \mu + 2t_x + 2t_y$ [13–16]. Reference [15] shows Majorana fermions may be generated in a 2D optical lattice with 1D ERD SOC along the x direction. This motivates us to demonstrate the existence of Majorana bound states in genuine 2D systems with 1D defects, where the SOC lays along $\vec{e}_x + \vec{e}_y$ direction. Through single-site addressing, a potential could be locally applied to a given site.

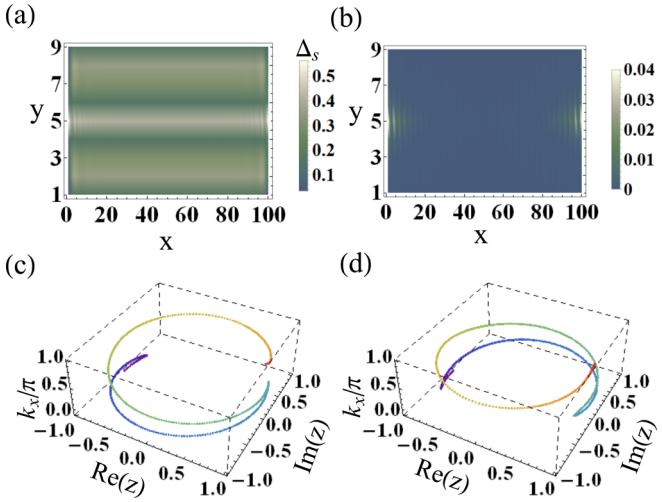

FIG. 6. (a) The amplitude of SF order parameter in real space. (b) The density distribution of the MZM. (c), (d) $z(k_x)$ in the complex plane for opposite winding number. In all panels we set $t_x = t_y = 1$, $h_z = 1.4$, $\mu = -8.0$, $\mu_d = -4$, $\Delta_s = 0.3$, and $\Delta_a = 0.11$. We choose $t_{\rm sox} = t_{\rm soy} = 2$ in (a–c) and $t_{\rm sox} = t_{\rm soy} = -2$ in (d).

Imposing a 1D potential dip μ_d, we have the following Hamiltonian:

$$\hat{H}_{\rm BdG} = \hat{H}_s + \sum_{i\in -} \mu_d \hat{c}_i^\dagger \hat{c}_i, \tag{A1}$$

where $i \in -$ denotes the sites (i_x, i_y) satisfying $i_y = n_{y_c}$. In self-consistent numerical calculations, we take a lattice with $n_x = 100$, $n_y = 9$, and $n_{y_c} = 5$ under open boundary conditions, where n_x and n_y denote the site number along the x and y directions. Figures 6(a) and 6(b) present self-consistent numerical results. Figure 6(b) shows a density profile of the zero-energy mode ($E \approx 10^{-4}$). It demonstrates the existence of MZMs even in a genuine 2D system. From self-consistent BdG numerical results, the SF order parameter is almost homogeneous along the x direction, as shown in Fig. 6(a). Thus with periodic boundary conditions, the system has a translation symmetry along the x direction so that momentum k_x is a good quantum number. The 2D optical lattice can be regarded as a layered 1D chain with transverse tunneling and SOC effects. The effective Hamiltonian is then written as

$$\begin{aligned} H_{\rm BdG}(k_x) = {} & \kappa_0 h_0(k_x) + \mu_d \kappa_c \sigma_0 \tau_z + \Delta_a \kappa_c \sigma_y \tau_y \\ & - t_y \kappa_x \sigma_0 \tau_z - t_{\rm soy} \kappa_y \sigma_y \tau_z. \end{aligned} \tag{A2}$$

Here the matrix κ acts on chain space, with κ_0 the identity matrix, $(\kappa_c)_{i,i} = 1$ for $i = n_{y_c}$ and 0 otherwise, $(\kappa_x)_{i,j} = 1$ for $|i - j| = 1$, and $(\kappa_y)_{i,i\mp1} = \mp i$ and 0 otherwise. The term proportional to μ_d (Δ_a) describes the dip potential (the SF order) difference between the central chain and other individual chains. The term proportional to t_y ($t_{\rm soy}$) describes the hopping (SOC) along the y direction. The following Hamiltonian,

$$\begin{aligned} h_0(k_x) = {} & (-2t_x \cos k_x - \mu)\sigma_0 \tau_z + 2t_{\rm sox} \sin k_x \sigma_y \tau_z \\ & + h_z \sigma_z \tau_z + \Delta_s \sigma_y \tau_y, \end{aligned} \tag{A3}$$

describes the original uniform individual 1D chain along the x direction. σ and τ are Pauli matrices acting on spin space and particle-hole space, respectively. The above BdG Hamiltonian $H_{\rm BdG}(k_x)$ has intrinsic particle-hole symmetry $\mathcal{P}$: $\mathcal{P}H_{\rm BdG}(k_x)\mathcal{P}^{-1} = -H_{\rm BdG}(-k_x)$ with $\mathcal{P} = \tilde{\tau}_x \mathcal{K}$, $\tilde{\tau}_x = \tau_x \sigma_0 \eta_0$, where σ_0 is the 2×2 identity matrix, η_0 is a $N_s \times N_s$ identity matrix acting on the lattice site space, and $\mathcal{K}$ is the complex conjugation. If the superfluid order parameter is real (or has a constant phase that can be eliminated by gauge transformations), the Hamiltonian preserves a generalized time-reversal symmetry $\mathcal{T}$: $\mathcal{T}H_{\rm BdG}(k_x)\mathcal{T}^{-1} = H_{\rm BdG}(-k_x)$ with $\mathcal{T} = \mathcal{K}$. The composite operation of $\mathcal{P}$ and $\mathcal{T}$ also leads to a chiral symmetry $\mathcal{C}$: $\mathcal{C}H_{\rm BdG}(k_x)\mathcal{C}^{-1} = -H_{\rm BdG}(k_x)$, with $\mathcal{C} = \mathcal{P}\mathcal{T} = \tilde{\tau}_x$. From the above symmetry analyses, the Hamiltonian belongs to the BDI class, characterized by a $\mathbb{Z}$ topological invariant (winding number).

The winding number w can characterize the topological properties of the BdG Hamiltonian (A2) [17]. Because the BdG Hamiltonian H_{BDG} has chiral symmetry, it can be transformed into an off-diagonal form in particle-hole space under a unitary transformation $U = e^{-i\frac{\pi}{4}\tau_y}$:

$$U H_{\rm BdG}(k_x) U^{-1} = \begin{pmatrix} 0 & \mathcal{B}(k_x) \\ \mathcal{B}^T(-k_x) & 0 \end{pmatrix}. \tag{A4}$$

Here $\mathcal{B}(k_x) = \mathcal{B}_1(k_x) - i\mathcal{B}_2$, where $\mathcal{B}_1(k_x) = (-2t_x \cos k_x - \mu)\kappa_0\sigma_0 + 2t_{\rm sox} \sin k_x \kappa_0 \sigma_y + h_z \kappa_0 \sigma_z + \mu_d \kappa_c \sigma_0 - t_y \kappa_x \sigma_0 - t_{\rm soy} \kappa_y \sigma_y$ and $\mathcal{B}_2 = (\Delta_s \kappa_0 \sigma_y + \Delta_a \kappa_c \sigma_y)$. The winding number is defined as [17]

$$w = -\frac{i}{\pi} \int_0^\pi \frac{dz}{z(k_x)}, \tag{A5}$$

where $z(k_x) = \det[\mathcal{B}(k_x)]/|\det[\mathcal{B}(k_x)]|$. As shown in Figs. 6(c) and 6(d) with $h_z > \sqrt{(\mu + 2t_x + 2t_y - \mu_d)^2 + \Delta_s^2}$, the complex value of $z(k_x)$ varies when k_x changes from 0 to π, indicating $|w| = 1$. By considering the trajectory of $z(k_x)$ in the complex plane as k_x changing from 0 to π, $z(k_x)$ moves from a point on the negatively real axis to the positive axis while crossing the imaginary axis exactly once. It is clear that the winding number $w = -1$ when $t_{\rm sox} > 0$ in topological phase, as shown in Fig. 6(c), and the winding number $w = +1$ when $t_{\rm sox} < 0$ in topological phase, as shown in Fig. 6(d). Namely, the sign of winding number for the one-dimensional region is determined by the sign of SOC in the topological phase.

APPENDIX B: LOW-ENERGY THEORY OF TOPOLOGICAL SUPERFLUIDS ON A DEFECTIVE RECTANGLE

Remarkably, from Eq. (7) the term $\Delta_{\rm edge}$ does not change sign, but the coefficient $\alpha(s)$ changes sign at two corners of the defective outer rectangular region. This will give rise to a Majorana pair at the corner where $\alpha(s)$ changes sign. Hereafter, we will give the analytic solutions of Majorana corner modes.

According to the particle-hole symmetry of $H_{\rm edge}$, i.e., $\{H_{\rm edge}, \sigma_y\tau_y\} = 0$, we have

$$H_{\rm edge}\sigma_y\tau_y = -\sigma_y\tau_y H_{\rm edge}. \tag{B1}$$

It can be concluded that if there exist zero-energy states of $H_{\rm edge}$, these states are also eigenstates of $\sigma_y\tau_y$. Therefore we assume the zero-energy wave functions in the "edge coordinate" s have the following forms:

$$\Psi_{0,+} = f_+(s)|y_+\rangle_\sigma|y_+\rangle_\tau + g_+(s)|y_-\rangle_\sigma|y_-\rangle_\tau, \tag{B2}$$

$$\Psi_{0,-} = f_-(s)|y_+\rangle_\sigma|y_-\rangle_\tau + g_-(s)|y_-\rangle_\sigma|y_+\rangle_\tau. \tag{B3}$$

Then we have $\sigma_y\tau_y\Psi_{0,\pm} = \pm\Psi_{0,\pm}$ and the Schrödinger equation at the corner between the edge I and II (corner $s = 0$) is $H_{\rm edge}\Psi_{0,+} = 0$. Using the eigenvector $\Phi = [f_+(s), g_+(s)]^T$, the above equation (B1) can be rewritten as

$$\left(t\partial_s^2 + i\alpha\partial_s\sigma_z + \mu_{\rm edge} - i\Delta_{\rm edge}\sigma_z + h_z\sigma_x\right)\Phi = 0. \tag{B4}$$

We assume $f_+(s) = A_+e^{-\eta_+ s}$, $g_+(s) = B_+e^{-\eta_+ s}$ $(s > 0)$ and write

$$(-it\eta_+^2\sigma_z + \alpha\eta_+ - i\mu_{\rm edge}\sigma_z - \Delta_{\rm edge} + h_z\sigma_y)\tilde{\Phi} = 0, \tag{B5}$$

with $\tilde{\Phi} = (A_+, B_+)^T$. According to the vanishing determinant of the above matrix, we obtain

$$\eta_+ = \frac{1}{2}\sqrt{-\frac{2\varkappa}{3} + \delta} - \frac{1}{2}\sqrt{-\frac{4\varkappa}{3a} - \delta + \zeta_+} > 0, \tag{B6}$$

where $\varkappa$, δ, a, and ζ_+ have been written explicitly in the main text. Then we have $A_+/B_+ = e^{i\phi_+}$ with

$$e^{i\phi_+} = \frac{h_z[-(t\eta_+^2 + \mu_{\rm edge}) + i(\alpha\eta_+ - \Delta_{\rm edge})]}{(t\eta_+^2 + \mu_{\rm edge})^2 + (\alpha\eta_+ - \Delta_{\rm edge})^2}. \tag{B7}$$

At last, we get the MZM $\Psi_{0,+}$ at the corner between edges I and II. Following a similar approach as in previous calculations, we can get another zero-energy solution $\Psi_{0,-} = C_-e^{-\eta_-|s|}(e^{i\frac{\phi_-}{2}}|y_+\rangle_\sigma \otimes |y_-\rangle_\tau + e^{-i\frac{\phi_-}{2}}|y_-\rangle_\sigma \otimes |y_+\rangle_\tau)$ with C_- the normalization constant, where

$$\eta_- = \frac{1}{2}\sqrt{-\frac{2\varkappa}{3} + \delta} + \frac{1}{2}\sqrt{-\frac{4\varkappa}{3a} - \delta + \zeta_-} > 0, \tag{B8}$$

$$e^{i\phi_-} = \frac{h_z[-(t\eta_-^2 + \mu_{\rm edge}) + i(\alpha\eta_- + \Delta_{\rm edge})]}{(t\eta_-^2 + \mu_{\rm edge})^2 + (\alpha\eta_- + \Delta_{\rm edge})^2}, \tag{B9}$$

and the coefficients $\varkappa$, δ, a, and ζ_- are listed in the main text. In summary, there are two Majorana modes (a Majorana corner pair) localized around the corner with the analytic solution given in Eq. (8). Regarding the corner between III and IV, there exists another SOC domain wall and we similarly have a Majorana pair there.

APPENDIX C: LOW-ENERGY THEORY OF TOPOLOGICAL SUPERFLUIDS ON A DEFECTIVE RING

The general Hamiltonian for a spin-orbit coupled Fermi gas with s-wave Cooper pairing is given by

$$H_{\rm r} = \frac{1}{2m_0}(\vec{k} - k_0\vec{\sigma})^2 - \mu\tau_z + h_z\sigma_z + \Delta_s\tau_x, \tag{C1}$$

where $\vec{k} = -i\vec{\nabla}$. Assuming spin $\vec{\sigma}$ is along x and neglecting the constant energy shift $k_0^2/(2m_0)$, we get the Hamiltonian in Eq. (10). In the polar coordinate,

$$\begin{pmatrix}\vec{i}\\ \vec{j}\end{pmatrix} = \begin{pmatrix}\cos\phi & -\sin\phi\\ \sin\phi & \cos\phi\end{pmatrix}\begin{pmatrix}\vec{e}_\rho\\ \vec{e}_\varphi\end{pmatrix}. \tag{C2}$$

The Laplace operator in Descartes and polar coordinates is written as

$$\vec{\nabla} = \partial_x\vec{i} + \partial_y\vec{j} = \partial_\rho\vec{e}_\rho + \frac{1}{\rho}\partial_\phi\vec{e}_\phi. \tag{C3}$$

Then we have $\vec{k}^2 = -\vec{\nabla}\cdot\vec{\nabla} = -(\partial_\rho^2 + \frac{1}{\rho^2}\partial_\phi^2)$ and

$$\vec{k}\cdot(\sigma_x\vec{i}) = -i\left[\cos\phi\partial_\rho + \frac{1}{\rho}\partial_\phi(-\sin\phi)\right]\sigma_x. \tag{C4}$$

Finally, Eq. (10) can be rewritten as the following form:

$$\begin{aligned}\mathcal{H} = \frac{1}{2m_0}\Bigg[&-\left(\partial_\rho^2 + \frac{1}{\rho^2}\partial_\phi^2\right) - ik_0\left(\cos\phi\partial_\rho - \frac{1}{\rho}\sin\phi\partial_\phi\right)\\ &\times\sigma_x - ik_0\left(\cos\phi\partial_\rho - \frac{1}{\rho}\sin\phi\partial_\phi\right)\sigma_x\Bigg]\tau_z - \mu\tau_z\\ &+ h_z\sigma_z + \Delta_s\tau_x.\end{aligned} \tag{C5}$$

Consider ultracold atoms trapped in a ring-shaped trapping potential, where the radii ρ is fixed. Terms with respect to ∂_ρ disappear. After substituting $\eta = \frac{1}{2m_0\rho^2}$, $\tilde{\alpha}_0 = \frac{k_0}{m_0\rho} = \frac{\alpha_0}{\rho}$, and $\mu' = \mu - \frac{k_0^2}{2m_0}$, the Hamiltonian $\mathcal{H}$ becomes Eq. (11).

Because $\mathcal{H}(\phi)$ is invariant under a $2n\pi$ rotation with n being an integer, we assume the wave functions take following form as $\Phi(\phi) = [u_a(\phi), u_b(\phi), u_c(\phi), u_d(\phi)]^T$, where

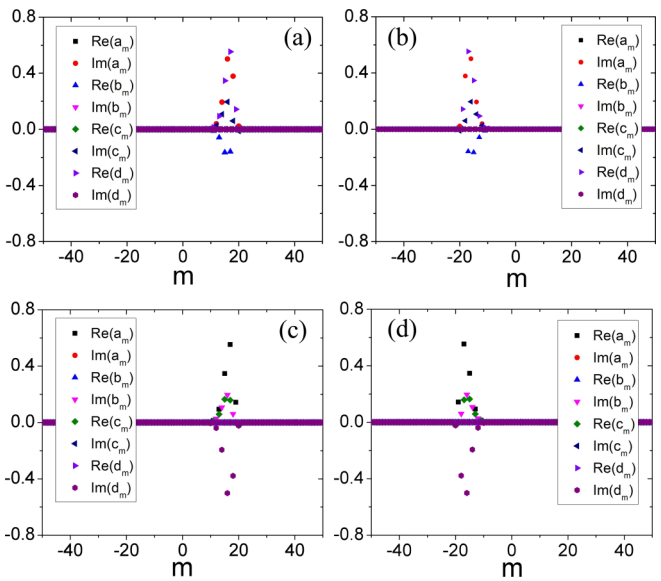

FIG. 7. The real and imaginary parts of coefficients (a_m, b_m, c_m, d_m) for the wave functions of four Majorana modes, respectively. The parameters $\tilde{\alpha}_0 = 0.04$, $\eta = 0.005$, $\mu' = 0.2$, $h_z = -1.4$, and $\Delta = 0.8$ are used for all panels.

$u_{v=a,b,c,d}(\phi) = \sum_{m=-N}^{N} v_m e^{im\phi}$. Plugging $\mathcal{H}(\phi)$ and $\Phi(\phi)$ into the Schrödinger equation $\mathcal{H}\Phi(\phi) = E\Phi(\phi)$, and matching coefficients for $e^{im\phi}$, one can obtain a series of coupled equations as

$$Ea_m = (\eta^2 m^2 - \mu' + h_z)a_m + i\frac{\tilde{\alpha}_0}{2}(m-1)b_{m-1} - i\frac{\tilde{\alpha}_0}{2}(m+1)b_{m+1} + \Delta_s c_m, \tag{C6}$$

$$Eb_m = \frac{i\tilde{\alpha}_0}{2}(m-1)a_{m-1} - i\frac{\tilde{\alpha}_0}{2}[m+1]a_{m+1} + (\eta m^2 - \mu' - h_z)b_m + \Delta_s d_m, \tag{C7}$$

$$Ec_m = \Delta_s a_m + [-\eta m^2 + \mu' + h_z]c_m - i\frac{\tilde{\alpha}_0}{2}(m-1)d_{m-1} + i\frac{\tilde{\alpha}_0}{2}(m+1)d_{m+1}, \tag{C8}$$

$$Ed_m = \Delta_s b_m - i\frac{\tilde{\alpha}_0}{2}(m-1)c_{m-1} + i\frac{\tilde{\alpha}_0}{2}(m+1)c_{m+1} + [-\eta m^2 + \mu' - h_z]d_m. \tag{C9}$$

By solving above coupled equations (C6)–(C9) with the truncation bounds for m up to 50, the eigenenergies and corresponding eigenfunctions $\Phi(\phi)$ could be obtained. Figure 5(c) in the main text presents the eigenspectrum, indicating that there are four Majorana zero modes. The coefficients v_m of wave functions of four Majorana modes are plotted in Fig. 7.

[1] C. Nayak, S. H. Simon, A. Stern, M. Freedman, and S. Das Sarma, Non-Abelian anyons and topological quantum computation, Rev. Mod. Phys. **80**, 1083 (2008).

[2] A. Y. Kitaev, Fault-tolerant quantum computation by anyons, Ann. Phys. **303**, 2 (2003).

[3] S. R. Elliott and M. Franz, Majorana fermions in nuclear, particle, and solid-state physics, Rev. Mod. Phys. **87**, 137 (2015).

[4] N. Read and D. Green, Paired states of fermions in two dimensions with breaking of parity and time-reversal symmetries and the fractional quantum Hall effect, Phys. Rev. B **61**, 10267 (2000).

[5] V. T. Phong, N. R. Walet, and F. Guinea, Majorana zero modes in a two-dimensional p-wave superconductor, Phys. Rev. B **96**, 060505(R) (2017).

[6] X.-L. Qi and S.-C. Zhang, Topological insulators and superconductors, Rev. Mod. Phys. **83**, 1057 (2011).

[7] M. Z. Hasan and C. L. Kane, Colloquium: Topological insulators, Rev. Mod. Phys. **82**, 3045 (2010).

[8] M. Sato, Y. Takahashi, and S. Fujimoto, Non-Abelian Topological Order in s-Wave Superuids of Ultracold Fermionic Atoms, Phys. Rev. Lett. **103**, 020401 (2009).

[9] C. Zhang, S. Tewari, R. M. Lutchyn, and S. Das Sarma, $p_x + ip_y$ Superfluid from s-Wave Interactions of Fermionic Cold Atoms, Phys. Rev. Lett. **101**, 160401 (2008).

[10] L. Jiang, T. Kitagawa, J. Alicea, A. R. Akhmerov, D. Pekker, G. Refael, J. I. Cirac, E. Demler, M. D. Lukin, and P. Zoller, Majorana Fermions in Equilibrium and in Driven Cold-Atom Quantum Chains, Phys. Rev. Lett. **106**, 220402 (2011).

[11] J. Alicea, Y. Oreg, G. Refael, F. von Oppen, and M. P. A. Fisher, Non-Abelian statistics and topological quantum information processing in 1D chain networks, Nat. Phys. **7**, 412 (2011).

[12] J. Alicea, New directions in the pursuit of Majorana fermions in solid state systems, Rep. Prog. Phys. **75**, 076501 (2012).

[13] Y. Oreg, G. Refael, and F. von Oppen, Helical Liquids and Majorana Bound States in Quantum Wires, Phys. Rev. Lett. **105**, 177002 (2010).

[14] R. M. Lutchyn, J. D. Sau, and S. Das Sarma, Majorana Fermions and a Topological Phase Transition in Semiconductor-Superconductor Heterostructures, Phys. Rev. Lett. **105**, 077001 (2010).

[15] L. Jiang, C. Qu, and C. Zhang, One-dimensional topological chains with Majorana fermions in two-dimensional nontopological optical lattices, Phys. Rev. A **93**, 063614 (2016).

[16] J. D. Sau, R. M. Lutchyn, S. Tewari, and S. Das Sarma, Generic New Platform for Topological Quantum Computation Using Semiconductor Heterostructures, Phys. Rev. Lett. **104**, 040502 (2010).

[17] S. Tewari and J. D. Sau, Topological Invariants for Spin-Orbit Coupled Superconductor Nanowires, Phys. Rev. Lett. **109**, 150408 (2012).

[18] T. Ojanen, Topological π Josephson junction in superconducting Rashba wires, Phys. Rev. B **87**, 100506(R) (2013).

[19] V. Mourik, K. Zuo, S. M Frolov, S. Plissard, E. Bakkers, and L. Kouwenhoven, Signatures of Majorana fermions in hybrid superconductor-semiconductor nanowire devices, Science **336**, 1003 (2012).

[20] A. D. K. Finck, D. J. Van Harlingen, P. K. Mohseni, K. Jung, and X. Li, Anomalous Modulation of a Zerobias Peak in a Hybrid Nanowire-Superconductor Device, Phys. Rev. Lett. **110**, 126406 (2013).

[21] S. Nadj-Perge, I. K Drozdov, J. Li, H. Chen, S. Jeon, J. Seo, A. H. MacDonald, B. A. Bernevig, and A. Yazdani, Observation of Majorana fermions in ferromagnetic atomic chains on a superconductor, Science **346**, 602 (2014).

[22] J.-P. Xu, M.-X. Wang, Z. L. Liu, J.-F. Ge, X. Yang, C. Liu, Z. A. Xu, D. Guan, C. L. Gao, D. Qian, Y. Liu, Q.-H. Wang, F.-C. Zhang, Q.-K. Xue, and J.-F. Jia, Experimental Detection of a Majorana Mode in the Core of a Magnetic Vortex inside a Topological Insulator-Superconductor $Bi_2Te_3/NbSe_2$ Heterostructure, Phys. Rev. Lett. **114**, 017001 (2015).

[23] Z. F. Wang, H. Zhang, D. Liu, C. Liu, C. Tang, C. Song, Y. Zhong, J. Peng, F. Li, C. Nie, L. Wang, X. J. Zhou, X. Ma, Q. K. Xue, and F. Liu, Topological edge states in a high-temperature superconductor FeSe/$SrTiO_3$ (001) film, Nat. Mater. **15**, 968 (2016).

[24] Q. L. He, L. Pan, A. L. Stern, E. Burks, X. Che, G. Yin, J. Wang, B. Lian, Q. Zhou, E. S. Choi, K. Murata, X. Kou, T. Nie, Q. Shao, Y. Fan, S.-C. Zhang, K. Liu, J. Xia, and K. L. Wang, Chiral Majorana edge state in a quantum anomalous Hall insulator-superconductor structure, Science **357**, 294 (2017).

[25] Y.-J. Lin, K. Jiménez-García, and I. B. Spielman, Spin-orbit-coupled Bose-Einstein condensates, Nature (London) **471**, 83 (2011).

[26] J.-Y. Zhang, S.-C. Ji, Z. Chen, L. Zhang, Z.-D. Du, B. Yan, G.-S. Pan, B. Zhao, Y.-J. Deng, H. Zhai, S. Chen, and J.-W. Pan,

Collective Dipole Oscillations of a Spin-Orbit Coupled Bose-Einstein Condensate, Phys. Rev. Lett. **109**, 115301 (2012).

[27] P. Wang, Z.-Q. Yu, Z. Fu, J. Miao, L. Huang, S. Chai, H. Zhai, and J. Zhang, Spin-Orbit Coupled Degenerate Fermi Gases, Phys. Rev. Lett. **109**, 095301 (2012).

[28] R. A. Williams, M. C. Beeler, L. J. LeBlanc, and I. B. Spielman, Raman-Induced Interactions in a Single-Component Fermi Gas Near an *s*-Wave Feshbach Resonance, Phys. Rev. Lett. **111**, 095301 (2013).

[29] L. Huang, Z. Meng, P. Wang, P. Peng, S.-L. Zhang, L. Chen, D. Li, Q. Zhou, and J. Zhang, Experimental realization of two-dimensional synthetic spin-orbit coupling in ultracold Fermi gases, Nat. Phys. **12**, 540 (2016).

[30] Z. Meng, L. Huang, P. Peng, D. Li, L. Chen, Y. Xu, C. Zhang, P. Wang, and J. Zhang, Experimental Observation of a Topological Band Gap Opening in Ultracold Fermi Gases with Two-Dimensional Spin-Orbit Coupling, Phys. Rev. Lett. **117**, 235304 (2016).

[31] Z. Wu, L. Zhang, W. Sun, X.-T. Xu, B.-Z. Wang, S.-C. Ji, Y. Deng, S. Chen, X.-J. Liu, J.-W. Pan, Realization of two-dimensional spin-orbit coupling for Bose-Einstein condensates, Science **354**, 83 (2016).

[32] A. Bühler, N. Lang, C. V. Kraus, G. Moller, S. D. Huber, and H. P. Büchler, Majorana modes and p-wave superfluids for fermionic atoms in optical lattices, Nat. Commun. **5**, 4504 (2014).

[33] D.-L. Deng, S.-T. Wang, K. Sun, and L.-M. Duan, Proposal for observing non-Abelian statistics of Majorana-Shockley fermions in an optical lattice, Phys. Rev. B **91**, 094513 (2015).

[34] J. Langbehn, Y. Peng, L. Trifunovic, F. von Oppen, and P. W. Brouwer, Reflection-Symmetric Second-Order Topological Insulators and Superconductors, Phys. Rev. Lett. **119**, 246401 (2017).

[35] W. A. Benalcazar, B. A. Bernevig, and T. L. Hughes, Quantized electric multipole insulators, Science **357**, 61 (2017).

[36] Z. Song, Z. Fang, and C. Fang, $(d-2)$-Dimensional Edge States of Rotation Symmetry Protected Topological States, Phys. Rev. Lett. **119**, 246402 (2017).

[37] C. Fang and L. Fu, Rotation anomaly and topological crystalline insulators, Sci. Adv. **5**, eaat2374 (2019).

[38] F. Schindler, A. M. Cook, M. G. Vergniory, Z. Wang, S. S. P. Parkin, B. A. Bernevig, and T. Neupert, Higher-order topological insulators, Sci. Adv. **4**, eaat0346 (2018).

[39] E. Khalaf, H. C. Po, A. Vishwanath, and H. Watanabe, Symmetry Indicators and Anomalous Surface States of Topological Crystalline Insulators, Phys. Rev. X **8**, 031070 (2018).

[40] X. Zhu, Tunable Majorana corner states in a two-dimensional second-order topological superconductor induced by magnetic fields, Phys. Rev. B **97**, 205134 (2018).

[41] E. Khalaf, Higher-order topological insulators and superconductors protected by inversion symmetry, Phys. Rev. B. **97**, 205136 (2018).

[42] Z. Yan, F. Song, and Z. Wang, Majorana Corner Modes in a High-Temperature Platform, Phys. Rev. Lett. **121**, 096803 (2018).

[43] Q. Wang, C.-C. Liu, Y.-M. Lu, and F. Zhang, High-Temperature Majorana Corner States, Phys. Rev. Lett. **121**, 186801 (2018).

[44] Y. Wang, M. Lin, and T. L. Hughes, Weak-pairing higher order topological superconductors, Phys. Rev. B **98**, 165144 (2018).

[45] T. Liu, J. J. He, and F. Nori, Majorana corner states in a two-dimensional magnetic topological insulator on a high-temperature superconductor, Phys. Rev. B **98**, 245413 (2018).

[46] C.-H. Hsu, P. Stano, J. Klinovaja, and D. Loss, Majorana Kramers Pairs in Higher-Order Topological Insulators, Phys. Rev. Lett. **121**, 196801 (2018).

[47] Z. Wu, Z. Yan, and W. Huang, Higher-order topological superconductivity: Possible realization in Fermi gases and Sr_2RuO_4, Phys. Rev. B **99**, 020508(R) (2019).

[48] Y. Xu, L. Mao, B. Wu, and C. Zhang, Dark Solitons with Majorana Fermions in Spin-Orbit-Coupled Fermi Gases, Phys. Rev. Lett. **113**, 130404 (2014).

[49] X.-J. Liu, Soliton-induced Majorana fermions in a one-dimensional atomic topological superfluid, Phys. Rev. A **91**, 023610 (2015).

[50] C. Zeng, T. D. Stanescu, C. Zhang, V. W. Scarola, and S. Tewari, Majorana Corner Modes with Solitons in an Attractive Hubbard-Hofstadter Model of Cold Atom Optical Lattices, Phys. Rev. Lett. **123**, 060402 (2019).

[51] P. Würtz, T. Langen, T. Gericke, A. Koglbauer, and H. Ott, Experimental Demonstration of Single-Site Addressability in a Two-Dimensional Optical Lattice, Phys. Rev. Lett. **103**, 080404 (2009).

[52] W. S. Bakr, J. I. Gillen, A. Peng, S. Folling, and M. Greiner, A quantum gas microscope for detecting single atoms in a Hubbard-regime optical lattice, Nature (London) **462**, 74 (2009).

[53] W. S. Bakr, A. Peng, M. E. Tai, R. Ma, J. Simon, J. I. Gillen, S. Foelling, L. Pollet, and M. Greiner, Probing the Superfluid-to-Mott insulator transition at the single-atom level, Science **329**, 547 (2010).

[54] J. F. Sherson, C. Weitenberg, M. Endres, M. Cheneau, I. Bloch, and S. Kuhr, Single-atom-resolved fluorescence imaging of an atomic Mott insulator, Nature (London) **467**, 68 (2010).

[55] C. Weitenberg, M. Endres, J. F. Sherson, M. Cheneau, P. Schauß, T. Fukuhara, I. Bloch, and S. Kuhr, Single-spin addressing in an atomic Mott insulator, Nature (London) **471**, 319 (2011).

[56] T. Köhler, K. Góral, and P. S. Julienne, Production of cold molecules via magnetically tunable Feshbach resonances, Rev. Mod. Phys. **78**, 1311 (2006).

[57] C. Chin, R. Grimm, P. Julienne, and E. Tiesinga, Feshbach resonances in ultracold gases, Rev. Mod. Phys. **82**, 1225 (2010).

[58] A. Altland and M. R. Zirnbauer, Nonstandard symmetry classes in mesoscopic normal-superconducting hybrid structures, Phys. Rev. B **55**, 1142 (1997).

[59] A. P. Schnyder, S. Ryu, A. Furusaki, and A. W. W. Ludwig, Classification of topological insulators and superconductors in three spatial dimensions, Phys. Rev. B **78**, 195125 (2008).

[60] A. Ramanathan, K. C. Wright, S. R. Muniz, M. Zelan, W. T. Hill III, C. J. Lobb, K. Helmerson, Superflow in a Toroidal Bose-Einstein Condensate: An Atom Circuit with a Tunable Weak Link, Phys. Rev. Lett. **106**, 130401 (2011).